2022 IEEE 5th International Conference on Soft Robotics (RoboSoft)
April 4-8, 2022, Edinburgh, UK

Whisker-based Haptic Perception System for Branch Detection in Dense Vegetation

Leiv Andresen[1], Emanuele Aucone[1,2] and Stefano Mintchev[1,2], *Member, IEEE*

***Abstract*— Dense vegetation is an example of a structurally complex environment that robots encounter in many outdoor applications such as agriculture, environmental monitoring, or search and rescue. For a robot to safely navigate or perform manipulation tasks in dense vegetation, it is important to detect and distinguish rigid branches from the surrounding soft foliage. This task is challenging for traditional sensing approaches, such as vision, because the foliage can partially or totally occlude the branches. We present a haptic sensing system capable of detecting contact with the vegetation and locating branches occluded by soft foliage. The system follows a vision-based tactile sensing approach consisting of an array of compliant whiskers, with fiducial markers attached to them, and a camera to track their displacement. When the whiskers are inserted in the vegetation and the array is oscillated, rigid branches cause the whiskers to deflect significantly, while deflections caused by softer foliage are smaller. We developed a sampling strategy and a software pipeline to detect the location of the branches based on the deflection magnitude of the whiskers. Upon indoor and outdoor experiments with artificial and natural vegetation, we demonstrate the ability to locate branches among compliant foliage.**

I. Introduction

Robotic platforms are increasingly deployed outside the controlled surroundings of factories and research facilities. Within several applications such as precision agriculture [1], environmental monitoring [2], [3], or search and rescue [4], robots often need to access and traverse regions with dense vegetation.

Robot navigation in dense vegetation is challenging because the surroundings are highly cluttered with unstructured obstacles, of which some are compliant (e.g., leaves) while others are rigid (e.g., thick branches). Additionally, the entire environment can move unpredictably due to wind. During missions within such an environment, leaves can be traversed, but to avoid fatal collisions robots need the ability to detect the network of rigid branches in the vegetation. However, in settings with dense foliage the branches are either not entirely visible from certain viewing angles or completely occluded. Furthermore, the dense nature of the vegetation creates a high dynamic range of lighting. As a result, branches become challenging to detect in images even with additional range information. There are promising approaches to estimate branch locations based on RGB-D data using learned image segmentation networks [5], [6], [7] but they are challenged in fully occluded settings. Alternatively, some laser scanners (LiDARs) are powerful enough to "shine" through foliage and record a secondary echo reflected from a branch [8]. However, aggregating these individual branch responses across scans is challenging and multi-beam laser scanners are generally too heavy and power consuming for lightweight platforms such as drones. These challenges motivate the exploration of alternative perception strategies to sense and understand the vegetation. Specifically, leveraging haptic perception, branches and foliage can be separated in the domain of compliance.

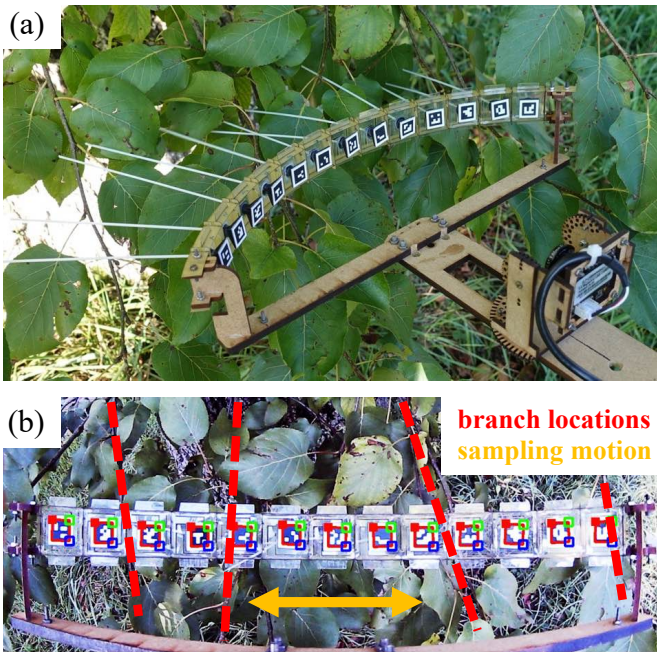

Fig. 1: The proposed haptic sensing system. (a) Prototype consisting of an array of soft artificial whiskers with fiducial markers that are tracked by a camera. (b) View from the camera while sampling vegetation to locate rigid branches among compliant foliage.

In the literature, haptic methods for surface type classification with force sensing feet have been used to estimate terrain traversability [9] and for localization [10]. Bioinspired whiskers are another promising approach to haptic perception in mobile robots [11], [12], [13], [14]. Whiskers that protrude from a robot can provide a pre-touch awareness by establishing contact with obstacles before the actual platform does. In addition to contact detection and localization, artificial whiskers can also provide information on the direction and amplitude of the interaction force [11].

[1]Environmental Robotics Laboratory, Department of Environmental Systems Science, Swiss Federal Institute of Technology Zurich, Switzerland smintchev@ethz.ch.
[2]Swiss Federal Institute for Forest, Snow and Landscape Research WSL, Birmensdorf, Switzerland.
This work was supported by the Swiss National Science Foundation through the research grant PCEFP2_186865.

2022 IEEE 5th International Conference on Soft Robotics (RoboSoft) | 978-1-6654-0828-8/22/$31.00 ©2022 IEEE | DOI: 10.1109/ROBOSOFT54090.2022.9762143

This makes it possible to detect branches based on the compliance of the vegetation. While advances in MEMS and nano-technology has enabled the miniaturization of tactile sensors and whiskers [15], [14] another approach, known as vision-based tactile sensing, leverages the miniaturization and performance of camera sensors [16]. In [17] an artificial finger-tip made of a rubber dome with internal protrusions is placed above a camera. When an object touches the dome from the outside the camera tracks the protrusions allowing algorithms to detect force interaction and identify shapes and textures. [18] presents a low-cost 6-DoF force and torque sensor using a camera that tracks fiducial markers attached to a platform suspended by springs. [19] presents 3D printed structures painted with different colours to track the bending and deformation of soft bodies with an RGB camera. These concepts have the benefit of decoupling the material interacting with the environment from the fragile sensing equipment. This improves the durability and simplifies the mechanical design and electrical wiring of such tactile sensors [16].

In this article we present a haptic system combining a vision-based tactile sensing approach with soft artificial whiskers for the detection and localization of rigid branches inside vegetation (Fig. 1a). The system consists of an array of passive whiskers mounted on a compliant support. Markers are connected to the whiskers and tracked with a camera. Once the whiskers are inside the vegetation, the array is translated left and right several times (see yellow arrow in Fig. 1b). The deflections of the whiskers during this whisking motion are recorded and processed to detect the location of the branches with respect to the whiskers.

Section II covers the working principle of the sensor, its design and the detection algorithm. Section III discusses experiments that were performed on a component and system level. A conclusion is drawn in the final section IV.

II. Implementation

The haptic sensing prototype consists of multiple whiskers incorporated into a rigid frame via an elastic coupling that allows the whiskers to be deflected by obstacles (Fig. 2a). Markers attached to each of the whiskers are tracked with a camera located in the center of the frame. The main concept is that obstacles can be detected and located by analyzing the displacements of the markers. Furthermore, these displacements provide a qualitative estimate of the direction and amplitude of the interaction force in the plane perpendicular to the whisker.

Branches are detected by entering inside the vegetation with an array of the proposed whiskers and moving the array in a repetitive motion (violet arrows, Fig. 2a), in the plane of the whiskers and perpendicular to the direction of entry. Rigid structures such as branches cause the whiskers to deflect significantly, while deflections caused by softer foliage are smaller. The location of the branches is estimated from the deflection data using a branch detection algorithm described in section II-B.

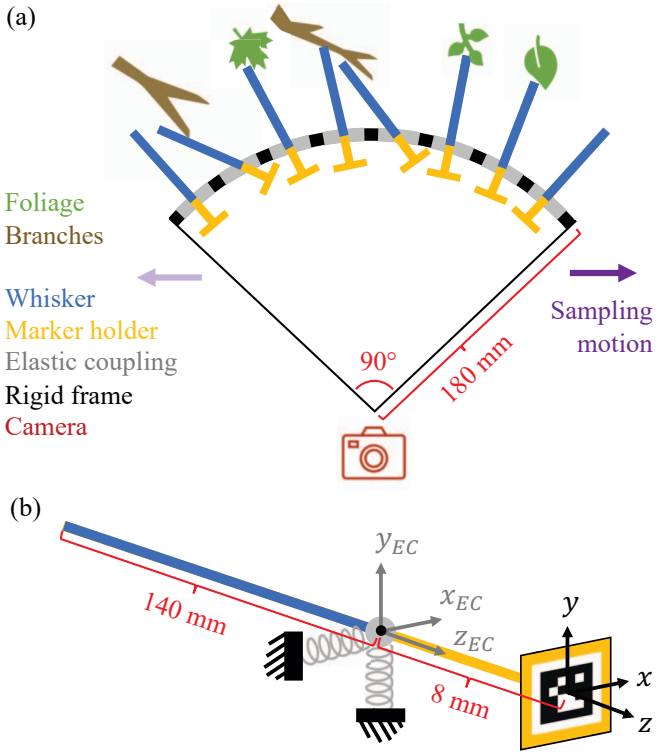

Fig. 2: The main concept and working principle of the haptic sensing system. (a) An array of soft whiskers is attached to a rigid frame via an elastic coupling; a marker is attached to the back of the whisker, and a camera is used to detect the deflections caused by the interaction with the surroundings. When the sensing system is moved (violet arrows) inside the vegetation, branches cause a higher deflection of the whiskers compared to foliage. (b) Schematics of a single whisker sensor showing the dimensions and coordinate frames.

A. Design and manufacturing

The components of the haptic sensing prototype (Fig. 3a) are i) a frame in the shape of a quadrant perimeter, ii) 13 equally spaced whiskers, which extend outside the frame to enter inside vegetation, iii) the elastic coupling connecting the whiskers to the frame (Fig. 3b), iv) the marker holder connecting the marker to the whisker (Fig. 3c, d), and v) the camera to track the markers.

The whiskers are made of 1.5 mm diameter polyester rods, which are industrially manufactured for brushes and recover a straight shape even after extensive bending. We chose a length of 140 mm which is approximately one third of the diameter of the circular array. A longer whisker increases the detection range at the cost of increasing the risk of unwanted entanglement in the vegetation.

The elastic coupling is a 2D spring obtained by laser cutting (*Trotec Speedy 360*) a square pattern on projector foil (*3M CG3300*, Fig. 3b). The spring acts as a torsional suspension that allows the whisker to rotate about the two axes perpendicular to the whisker at the elastic coupling (x_{EC} and y_{EC} in Fig. 2b). The spring is designed to be significantly softer than the whisker so the whisker's deflections get translated to traceable translations and rotations of the marker. On the other hand, the coupling is stiff

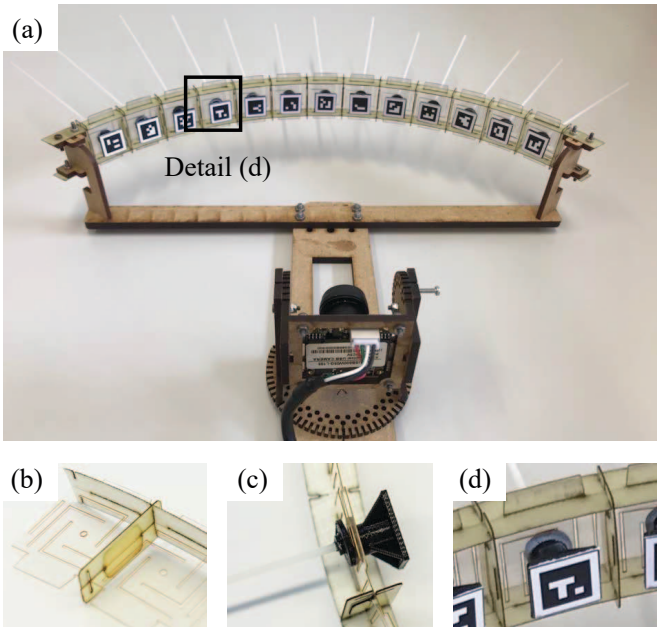

Fig. 3: The haptic sensing prototype. (a) It comprises 13 whiskers attached to a rigid frame via an elastic coupling made of projector foil (b, c); the camera is connected to the frame with a wooden structure and tracks the ArUco markers on the end of the whiskers (d).

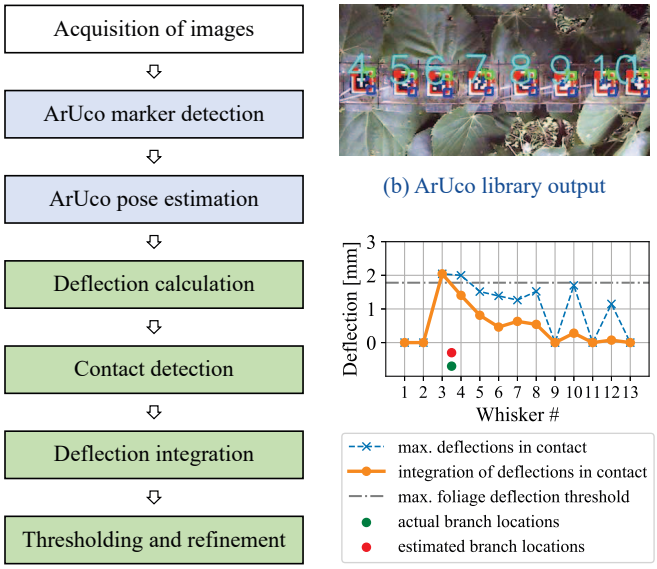

Fig. 4: Software pipeline overview. (a) Flowchart of the implemented software, (b) the ArUco marker detection and pose estimation, and (c) an exemplary output of the branch detection algorithm.

enough (approx. 5.7 Nmm/rad) to prevent deflections due to gravity, and due to movements and vibrations during transport. As discussed in the result section, the stiffness of the elastic coupling is an important design parameter that significantly affects the performance of the sensor: a stiffer coupling filters the foliage deflections more efficiently at the cost of reduced sensitivity and higher risk of entanglement.

Markers and their detection are provided by the widely used ArUco library which has built-in pose estimation and superior runtime performance compared to other squared fiducial markers [20]. The camera (*ELP-USB500W05G-L156*) records 5 megapixel videos at 15 fps with a lens field of view exceeding 180°. It is easy to integrate on a robot, as it weighs 30 grams, measures 32x32 cm, and interfaces via USB 2.0. Based on experiments to determine the marker detectability described in section III-A we chose markers of size 13.2 mm, from the official ArUco 4x4 bit dictionary. We observed that the marker rotation estimate provided by the ArUco library is not precise enough to use for the estimation of the whisker deflection, instead we use the marker translation estimate. This necessitates a rigid connection between the array of whiskers and the camera to prevent false deflection readings. The distance between the marker and the elastic coupling was set at 8 mm to provide a marker translation that can be detected accurately by the camera (maximum deflection of ∼7.5 mm). Increasing the distance would increase the deflection sensitivity but decrease the amount of whiskers that could be placed beside each other because the markers could collide.

B. Branch detection algorithm

The following section presents the algorithm used to detect branches. Fig. 4a illustrates the sensing software that starts with the acquisition of images (at 15 fps) while the array of 13 whiskers enters the vegetation and performs a periodic translatory movement (violet arrows in Fig. 2a). All the data acquired in one sampling process is referred to as a sample. The ArUco marker detection and pose estimation is performed on every image of the sample (Fig. 4b), providing the input data for the branch detection pipeline.

1) Deflection calculation: To detect a contact and perform branch detection we want an estimate of the whisker's pose after deflection (M), relative to its initial, *no-contact* pose (M_0). We denote this pose difference with the transformation T_{M_0M}. The ArUco library provides an estimate of the marker pose in the frame of the camera C, corresponding to the transformation T_{CM}. A *no-contact* transformation T_{CM_0} is initialized online while not in contact with the surroundings. This transformation is not hard-coded based on the ground-truth position of the markers because the estimation is not perfectly accurate and the exact setup may change slightly between deployments. Given T_{CM_0} and the transformation from the camera to the current deflected marker frame T_{CM}, we can reconstruct the desired transformation as:

$$T_{M_0M} = T_{CM_0}^{-1} * T_{CM} \tag{1}$$

The transform T_{M_0M} is acquired for every whisker in every camera image in the sample. Thereafter, the x and y translation components are extracted and the absolute deflection is calculated as $\sqrt{x^2+y^2}$ (referred to as "deflection" for the remainder of this work).

2) Contact detection: A deflection is classified as a contact if it exceeds a certain threshold. Several qualitative tests showed that a minimum threshold of 1 mm can filter unwanted deflections due to abrupt movements of the sensor, which are significantly larger than the estimation noise.

However, deflections above this minimum threshold could occur if the sensor is integrated on a moving robot and the whisker oscillates heavily. To filter these cases, a deflection is only classified as a contact if the mean deflection vector of the past four measurements exceeds the threshold.

3) Deflection integration: Given the deflection over time for each whisker, we aim to reduce the three-dimensional data to a one-dimensional estimate of the branch location along the array of whiskers. Reducing the time dimension by taking the maximum value of the deflection for every whisker leads to ambiguous results since it does not take into account the duration of the deflections. Of all the strategies we evaluated - mean, median, Laplacian and Gaussian filters - integrating (taking the sum of) the deflections for each whisker, when they are in contact, proved to be the most effective in amplifying the branch response. The absolute value of the integration depends on the specific execution of the whisking motion; hence, it is not comparable across samples. Therefore, the integration values are scaled to fit the maximum deflection values. The integration values of all whiskers form a curve and the peaks thereof represent branch location estimates.

4) Thresholding and refinement: Although the integration of deflections amplifies the prolonged deflections caused by branches, secondary peaks can remain in the integration curve. A deflection threshold is defined to filter these false positive peaks. An intuitive value for this threshold is to set it at the highest deflection measured when sampling foliage without any branches. We refer to this threshold as *maximum foliage deflection threshold*. A whisker is only a candidate for a branch location estimate if we measure a maximum deflection or scaled deflection integration value higher than this threshold. Finally, we perform a refinement of the branch location estimate because deflection integration peaks are located at a single whisker, whereas a branch is located in between two whiskers. By looking at the directionality of the deflection we can infer which side of the whisker the branch is located at. During the sampling process the whisker to the left of a branch will be deflected to the left as the branch moves towards it and vice-versa for the whisker on the right. This behavior is reflected in the displacement along the x axis of the *no-contact* marker frame (which is aligned with the plane of the sampling motion). The branch is most likely to be between two whiskers with a negative difference in x-deflection integration value because this means that these two whiskers were pushed apart.

5) Exemplary output: Fig. 4c depicts the final output of the branch detection algorithm for an exemplary sample with one branch, located between whiskers #3 and #4 (denoted with a green dot). For each of the 13 whisker the maximum deflection in contact (blue dashed line) and the deflection integration (orange line) is shown. The integration curve amplifies whiskers with prolonged deflections that indicate contact with branches, thereby differentiating them from whiskers with high momentary deflections that could stem from foliage. The *maximum foliage deflection threshold* is drawn as a grey horizontal line and filters the branch location estimates (deflection integration peaks) at whiskers #7, #10 and #12. Finally the red dot indicates the remaining branch location estimate which has been shifted from the peak at whisker #3 by the refinement step.

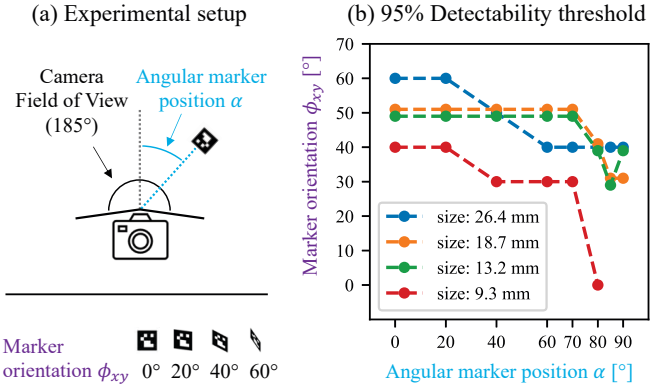

Fig. 5: Marker detectability experiment. (a) Illustration of the experimental parameters: angular marker position and marker orientation. (b) Most extreme marker orientations for which the marker was detected in at least 95% of the images vs. angular marker position. The four lines correspond to four marker sizes.

III. Experimental Results

This section discusses experiments that were performed to find a suitable marker size as well as branch detection experiments with artificial and real vegetation, both indoor and outdoor.

A. ArUco marker detection

A quantitative experiment was performed to determine the size of the ArUco markers. The ArUco pipeline starts with a marker detection step in which the image is preprocessed, the square marker is localized and the unique binary pattern inside it is resolved [20]. Subsequently the pose of the marker is estimated given the location of the marker's corners and the marker's size [21]. Theoretically, larger markers are easier to detect and provide better pose estimates, with the drawback of increasing the space needed between two whisker sensors. To investigate the detectability, markers of various sizes were placed at eight different angular positions α in the camera's field of view (Fig. 5a, α [°] = 0, 20, 40, 60, 70, 80, 85, 90), reaching beyond the range of our haptic sensing prototype (45°) for generality. At each angular position the markers were placed in eight different orientations ϕ_{xy}: starting with an orientation facing the camera the marker was rotated about the two axes in the marker plane (x and y axes in Fig. 2b) by the same angle (Fig. 5a, ϕ_{xy} [°] = 0, 10, 20, ... 70). For each combination of angular position and orientation, 60 images were acquired.

Fig. 5b shows the results for markers of four sizes. For each angular marker position on the x-axis, the y-axis indicates the highest marker orientation ϕ_{xy} for which the marker was detected in at least 95% of the 60 images. All markers are taken from the official ArUco 4x4 bit dictionary. We observe that the smallest marker is not detected for angular positions exceeding 80°. However, the remaining sizes are detected, even at angular positions close to the

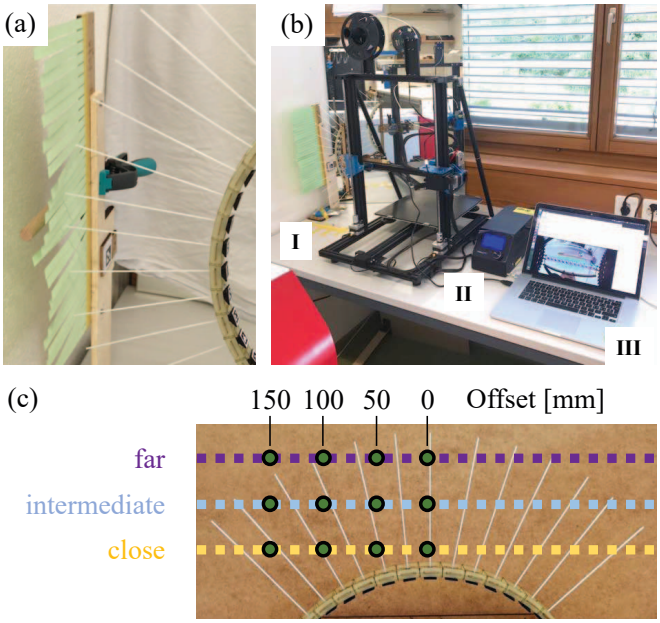

Fig. 6: Indoor testing. (a) Artificial vegetation with paper-made foliage and wooden rod as a branch. (b) Experimental setup with I) artificial vegetation, II) 3D printer, and III) laptop. (c) Illustration of the sampling distances and branch locations. For each sampling distance, the branches are placed at the center and with an offset of 50, 100 and 150 mm (green dots).

edge of the camera's field of view. The fact that the largest marker does not consistently outperform the intermediate ones could be due to it experiencing more distortion or the specific pattern being resolved less reliably. We decided to use markers of size 13.2 mm for our application.

Considering the pose estimation performance for this marker size, we observed that the rotation estimate provided by the ArUco library showed errors of up to 17° whereas the translation component was estimated with errors as high as 0.5 mm. While the marker rotation directly corresponds to the whisker's angular deflection, the marker translation relates to the deflection via the distance between the marker and the elastic coupling. In our setup with a distance of 8 mm, using the translation estimate gives a significantly lower maximum rotational error of 3.6°.

B. Branch detection with artificial vegetation

For an initial set of experiments to validate the detection of rigid structures behind a compliant occlusion, we developed a setup to simulate compliant foliage and rigid branches (Fig. 6a). The foliage was made of paper that was cut into stripes by a laser-cutter; the branches were modeled by a round, wooden rod with a diameter of 10 mm. The array of whiskers was attached to the vertical axis of a *Creality* 3D printer to perform the whisking motion repeatably. The camera was connected to a laptop on which the branch detection software was executed (Fig. 6b).

The goal of the experiments was to validate the branch detection algorithm, and understand the influence of the following parameters on the branch detection performance: foliage stiffness, sampling distance, and branch locations. The whisking motion consisted of two translations of $\pm$ 50 mm,

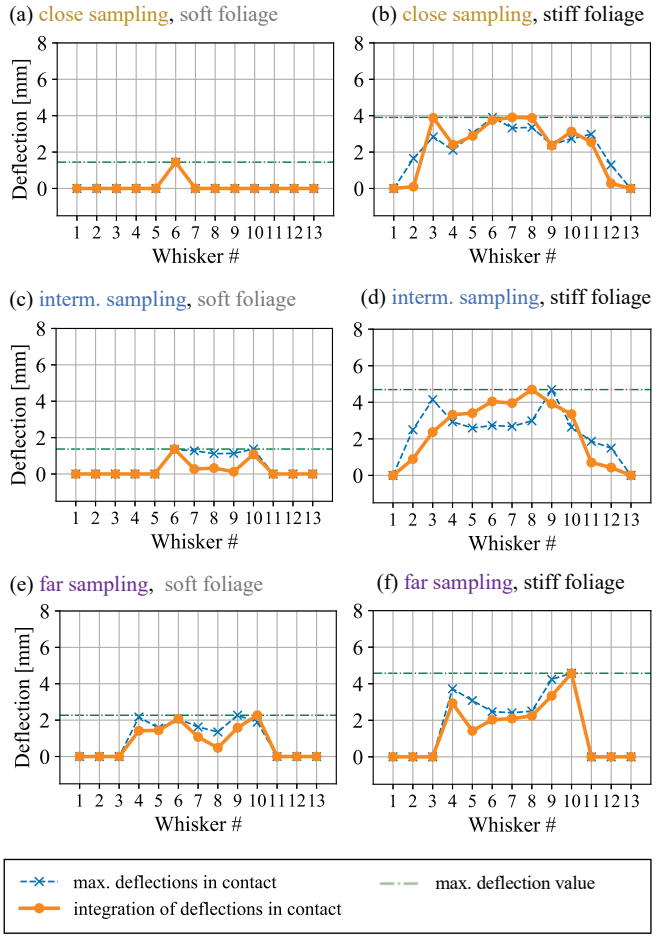

Fig. 7: Sampling response for soft and stiff artificial foliage without branches, sampled at various distances.

which is enough to ensure a branch centered between two whiskers causes a significant deflection when it comes in contact. Increasing the amplitude of the whisking motion increases the risk that the whiskers "skip" past branches, complicating the branch localization process. The speed of the whisking motion was approximately 4 mm/s. The motion was performed at three different sampling distances: *far*, *intermediate* and *close*. For each sampling distance, branches were placed at various locations: in the center and with a 50, 100 and 150 mm offset (Fig. 6c). Two different thicknesses of paper were tested to analyze the influence of the stiffness of the foliage: a thinner paper referred to as "soft" (80 g/cm^2) and a thicker paper referred to as "stiff" (160 g/cm^2).

1) Foliage response: Initially, both the soft and stiff artificial model of foliage was sampled without any branches behind it, in order to establish the deflection levels caused by the "leaves". As expected the maximum deflections are higher for the stiff foliage (Fig. 7b, d, f). Furthermore, for the soft foliage we observe that the deflections increase with increasing sampling distance (Fig. 7a, c, e). An explanation for this behavior is that the elastic coupling behaves like a torsional spring: the deflection is proportional to the torque applied to the spring. The foliage can withstand a certain force before it is pushed aside and that force causes a

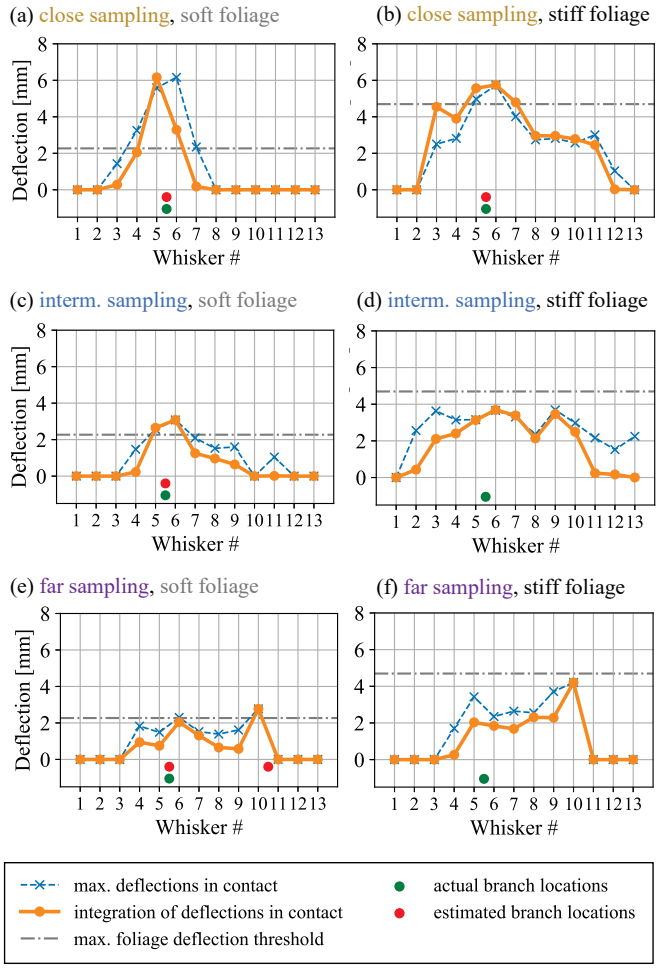

Fig. 8: Output of the branch detection algorithm for samples with a single branch placed 50 mm off center, behind soft and stiff foliage and sampled at various distances.

higher torque when it is applied farther from the base. This indicates that the whisker array has a varying force sensitivity: it is more sensitive to forces at the ends of the whiskers than at the base. The effect is visible for the stiff foliage as well: due to the curved shape of the sensor we can tell that the whiskers off center show higher maximum deflections for the *intermediate* and *far* sampling distances (dashed blue lines in Fig. 7d, f). Although high sensitivity is useful for detecting softer vegetation, the disadvantage is that stiffer foliage can saturate the sensor by causing large deflections when sampled with the tip of the whisker. This is a problem because branches cannot be detected if the sensor is saturated by the foliage. In this scenario, the deflections from the foliage can be seen as background noise that shall be minimised, while the deflections caused by the branches correspond to the signal we want to detect. The *maximum foliage deflection threshold* (described in section II-B.4) attempts to filter this background noise on an algorithmic level. It is set to the maximum deflection values that were recorded while sampling the respective foliage, disregarding the varying sensitivity for simplicity and robustness.

2) Branch detection with individual branches: Consequently, individual branches were placed at various positions

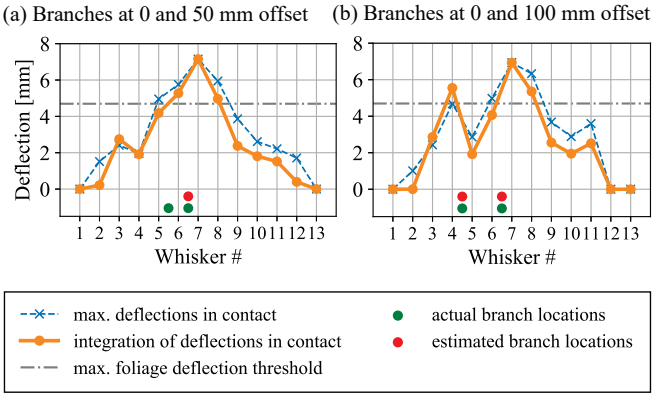

Fig. 9: Output of the branch detection algorithm for samples with two branches placed in the center and at 50 mm or 100 mm off center, behind stiff foliage and sampled at *close* distance.

behind the respective foliage. To illustrate the findings of the multitude of experiments we present the results for one of the branch configurations: Fig. 8 shows the sampling responses for a single artificial branch placed behind the artificial foliage 50 mm off center. Looking at the plots for the soft foliage (Fig. 8a, c, e) we observe a distinct response and correct estimates for both the *close* and *intermediate* sampling distance. For *far* sampling distance the branch response is not high enough to cross the threshold and not distinct, since there is a false positive branch detection due to a high foliage deflection. Concerning the stiff artificial foliage (Fig. 8b, d and f) only the *close* sampling distance gives a response above the foliage threshold, with an additional peak very close to the threshold at whisker #3. For the *intermediate* and *far* sampling distances the response remains under the threshold and is also not distinct: a lower threshold would lead to a false positive detection at whisker #9 or #10 respectively.

The fact that closer sampling gives better results can be explained by observing that with a constant amplitude of the whisking motion, a rigid obstacle causes greater deflections when it comes in contact with a whisker near the elastic coupling. This kinematic amplification, in conjunction with the reduced foliage sensitivity of closer sampling (see section III-B.1), leads to successful branch detection for *close* and *intermediate* sampling distances for soft foliage and *close* sampling distance for stiff foliage.

3) Branch detection with multiple branches: We proceeded to assess the haptic sensors' ability to discriminate multiple branches. We observe that if two branches are located close to each other, such that there is only one whisker between them, the algorithm cannot discern the individual branches. Fig. 9a illustrates this finding for two branches placed at 0 and 50 mm offset behind stiff foliage and sampled at *close* distance. Arguably, this is not a drawback from a practical perspective, because two branches so close together are similar to one thicker branch. The branches are discriminated as soon as there are at least two whiskers between them, as shown in Fig. 9b with branches placed at 0 and 100 mm offset. Additionally we observe that the branch response decreases when the branch is located farther away

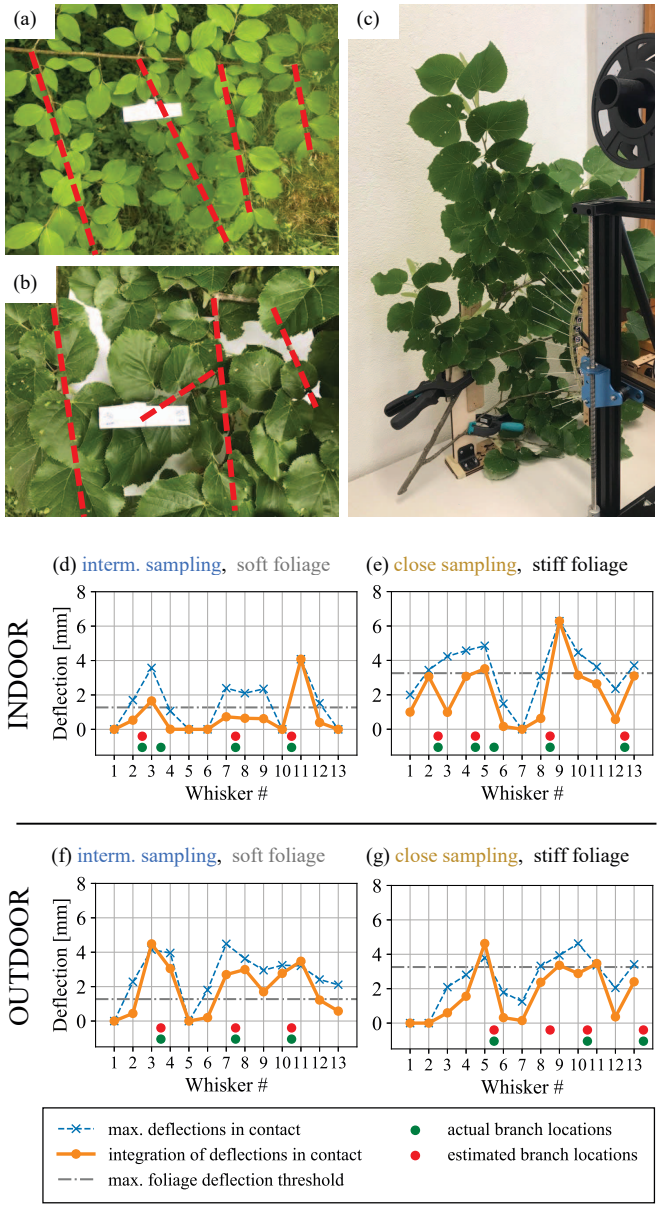

Fig. 10: Experiments with real vegetation. (a) *Cornus mas*, soft and relatively sparse leaves. (b) *Tilia tomentosa*, stiffer and denser foliage. Dashed lines = branch locations. (c) *Tilia tomentosa* mounted on the indoor experimental setup. (d)-(g) Branch detection algorithm output for real vegetation sampled indoors and outdoors.

from the center. This is due to the curved shape of the array of whisker and the aforementioned kinematic amplification of deflections close to the whiskers' base.

C. Branch detection with real vegetation

After the controlled experiments with artificial vegetation the findings were validated with real branches, both indoors and outdoors. The two types of vegetation (Fig. 10a, b) that were selected for the experiments are relatively planar and, in the case of Fig. 10b, branch locations are not trivial for an algorithm to detect visually or with depth information.

1) Indoor experiment: The real branches were attached to a stand (Fig. 10c) and the sampling procedure used for the artificial vegetation was repeated. To establish the *maximum foliage deflection threshold*, the whisking motion was performed parallel to a branch so that the whiskers were only in contact with the foliage. The results of the indoor experiments show a successful branch detection performance for the soft foliage. For the *close* (not shown) and *intermediate* (Fig. 10d) sampling distances, all branches are repeatedly detected correctly, without false positives, except for two branches that were too close to each other. Concerning the stiff foliage, we observe that for the *close* sampling distance (Fig. 10e) all branches are detected correctly, except the branch between whisker #5 and #6, again because it is too close to the other branch. Analogous to the results with artificial, stiff vegetation, we observe false negatives and positives when sampled at *intermediate* distance (not shown).

2) Outdoor experiment: For the outside experiments the whisking motion was performed by hand and the sampling distance was measured with a ruler. Differing from the controlled indoor experiments, the whisking motion of $\pm$ 50 mm was accelerated (80 mm/s as opposed to 4 mm/s) to prevent the entire branch from moving and was performed three times instead of two, to acquire sufficient data. Both vegetation types were sampled several times for each sampling distance.

As expected based on the previous results, the experiment showed that the branch detection algorithm is successful for the vegetation with soft foliage both at *close* (not shown) and *intermediate* (Fig. 10f) sampling distance. However the detection is not successful for the vegetation with stiff foliage. Fig. 10g shows a representative result: the stiff foliage does not feature a distinct response as there is a false positive estimation.

IV. Conclusions

In this work, we presented a haptic sensing system integrating artificial whiskers and a vision-based tactile sensing approach to detect the location of branches occluded by foliage. In summary, our setup performed well for vegetation with soft foliage both in artificial and natural scenarios. Branches are detected correctly as long as the whiskers enter the vegetation at least halfway (*close* and *intermediate* sampling distance). On the other hand, branches occluded by stiffer foliage are correctly detected only in controlled indoor tests with a *close* sampling distance. Table I gives an overview of all the results described in the previous sections:

Foliage stiffness	**soft**		**stiff**	
Sampling distance	*close*	*interm.*	*close*	*interm.*
Vegetation				
Artificial, indoor				
Real, indoor				
Real, outdoor				

TABLE I: Summary of the branch detection performance across various sampling settings and vegetation types. A green box indicates correct branch detection, whereas a red box indicates an output with false positive or false negative detections.

Our results show a trade-off between sensitivity and detectability of branches. With the decision to mount the whiskers on an elastic coupling with low torsional stiffness

(approx. 5.7 Nmm/rad), we developed whiskers with high sensitivity that can detect very soft vegetation. However, the deflections caused by stiffer foliage can be so high that the sensor saturates. As discussed in the end of sections III-B.1 and III-B.2, deflections caused by the foliage can be seen as background noise that can saturate the sensor, thus preventing branch detection. With the current setup, this problem is mitigated by sampling at a close distance from the base of the whiskers, which provides a kinematic amplification of the deflections caused by the rigid branches (i.e., the signal to noise ratio of the sensor is increased).

Future work could investigate the development of variable stiffness whiskers where the trade-off between sensitivity and saturation can be optimally tuned according to the mechanical properties of the vegetation. Furthermore, the stiffness of the foliage is currently recorded in advance to set a threshold for the algorithm to filter the foliage noise, but in the future this threshold could be inferred online. Alternatively, the stiffness of the whiskers and the threshold could be informed by a task, e.g., they are adjusted such that the whiskers do not detect a branch when in contact with traversable vegetation.

Concerning the vision-based deflection estimation, robustness could be improved with a more precise estimate of the marker rotation. Therefore, future work could investigate using alternative markers [22] or panoramic camera calibration models for the ArUco marker pose estimation [23].

Extensions of this work could investigate integrating the existing haptic system on terrestrial and aerial robots to perform branch detection on-board. The segment of whiskers could be extended to an entire circular band to provide a robot with 360° of contact awareness (in the plane of longitudinal and lateral motion) for collision avoidance, navigation, or mapping.

REFERENCES

[1] S. Asseng and F. Asche, "Future farms without farmers," *Science Robotics*, vol. 4, no. 27, p. eaaw1875, Feb. 2019.

[2] L. F. P. Oliveira, A. P. Moreira, and M. F. Silva, "Advances in Forest Robotics: A State-of-the-Art Survey," *Robotics*, vol. 10, no. 2, p. 53, Mar. 2021.

[3] S. Kirchgeorg and S. Mintchev, "HEDGEHOG: Drone Perching on Tree Branches With High-Friction Origami Spines," *IEEE Robotics and Automation Letters*, vol. 7, no. 1, pp. 602–609, 2021.

[4] J. Delmerico, S. Mintchev, A. Giusti, B. Gromov, K. Melo, T. Horvat, C. Cadena, M. Hutter, A. Ijspeert, D. Floreano, L. M. Gambardella, R. Siegwart, and D. Scaramuzza, "The current state and future outlook of rescue robotics," *Journal of Field Robotics*, vol. 36, no. 7, pp. 1171–1191, Oct. 2019.

[5] S. Tejaswi Digumarti, L. M. Schmid, G. M. Rizzi, J. Nieto, R. Siegwart, P. Beardsley, and C. Cadena, "An Approach for Semantic Segmentation of Tree-like Vegetation," in *2019 International Conference on Robotics and Automation (ICRA)*. Montreal, QC, Canada: IEEE, May 2019, pp. 1801–1807.

[6] Z. Chen, D. Ting, R. Newbury, and C. Chen, "Semantic segmentation for partially occluded apple trees based on deep learning," *Computers and Electronics in Agriculture*, vol. 181, p. 105952, Feb. 2021.

[7] W. Ji, X. Meng, Z. Qian, B. Xu, and D. Zhao, "Branch localization method based on the skeleton feature extraction and stereo matching for apple harvesting robot," *International Journal of Advanced Robotic Systems*, vol. 14, 2017.

[8] S. Hsu, S. Samarasekera, and R. Kumar, "Automatic registration and visualization of occluded targets using ladar data," G. W. Kamerman, Ed., Orlando, FL, Aug. 2003, p. 209.

[9] H. Kolvenbach, C. Bartschi, L. Wellhausen, R. Grandia, and M. Hutter, "Haptic Inspection of Planetary Soils With Legged Robots," *IEEE Robotics and Automation Letters*, vol. 4, no. 2, pp. 1626–1632, Apr. 2019.

[10] R. Buchanan, J. Bednarek, M. Camurri, M. R. Nowicki, K. Walas, and M. Fallon, "Navigating by touch: haptic Monte Carlo localization via geometric sensing and terrain classification," *Autonomous Robots*, Aug. 2021.

[11] T. Prescott, M. Pearson, B. Mitchinson, J. Sullivan, and A. Pipe, "Whisking with robots," *IEEE Robotics & Automation Magazine*, vol. 16, no. 3, pp. 42–50, Sept. 2009.

[12] C. Papachristos, S. Khattak, and K. Alexis, "Haptic Feedback-Based Reactive Navigation for Aerial Robots Subject to Localization Failure," in *2019 IEEE Aerospace Conference*. Big Sky, MT, USA: IEEE, Mar. 2019, pp. 1–7.

[13] A. Tagliabue, A. Paris, S. Kim, R. Kubicek, S. Bergbreiter, and J. P. How, "Touch the Wind: Simultaneous Airflow, Drag and Interaction Sensing on a Multirotor," in *2020 IEEE/RSJ International Conference on Intelligent Robots and Systems (IROS)*. Las Vegas, NV, USA: IEEE, Oct. 2020, pp. 1645–1652.

[14] W. Deer and P. E. I. Pounds, "Lightweight Whiskers for Contact, Pre-Contact, and Fluid Velocity Sensing," *IEEE Robotics and Automation Letters*, vol. 4, no. 2, pp. 1978–1984, Apr. 2019.

[15] P. S. Girão, P. M. P. Ramos, O. Postolache, and J. Miguel Dias Pereira, "Tactile sensors for robotic applications," *Measurement*, vol. 46, no. 3, pp. 1257–1271, Apr. 2013.

[16] A. Yamaguchi and C. G. Atkeson, "Recent progress in tactile sensing and sensors for robotic manipulation: can we turn tactile sensing into vision?" *Advanced Robotics*, vol. 33, no. 14, pp. 661–673, July 2019.

[17] B. Winstone, G. Griffiths, T. Pipe, C. Melhuish, and J. Rossiter, "TACTIP - Tactile Fingertip Device, Texture Analysis through Optical Tracking of Skin Features," in *Biomimetic and Biohybrid Systems*. Berlin, Heidelberg: Springer Berlin Heidelberg, vol. 8064.

[18] R. Ouyang and R. Howe, "Low-Cost Fiducial-based 6-Axis Force-Torque Sensor," *arXiv:2005.14250 [cs]*, May 2020, arXiv: 2005.14250.

[19] K. Hanaoka, M. Shimizu, and T. Umedachi, "Development of 3D Printed Structure that Visualizes Bending and Compression Deformations for Soft-bodied Robots," in *2021 IEEE 4th International Conference on Soft Robotics (RoboSoft)*, apr 2021, pp. 155–162.

[20] F. J. Romero-Ramirez, R. Muñoz-Salinas, and R. Medina-Carnicer, "Speeded up detection of squared fiducial markers," *Image and Vision Computing*, vol. 76, pp. 38–47, Aug. 2018.

[21] S. Garrido-Jurado, R. Muñoz-Salinas, F. Madrid-Cuevas, and M. Marín-Jiménez, "Automatic generation and detection of highly reliable fiducial markers under occlusion," *Pattern Recognition*, vol. 47, no. 6, pp. 2280–2292, 2014.

[22] H. Tanaka, Y. Sumi, and Y. Matsumoto, "A high-accuracy visual marker based on a microlens array," in *2012 IEEE/RSJ International Conference on Intelligent Robots and Systems*, 2012, pp. 4192–4197.

[23] J. Hajjami, J. Caracotte, G. Caron, and T. Napoleon, "ArUcOmni: detection of highly reliable fiducial markers in panoramic images," in *2020 IEEE/CVF Conference on Computer Vision and Pattern Recognition Workshops (CVPRW)*. Seattle, WA, USA: IEEE, June 2020, pp. 2693–2699.